

Tuning the electronic transport anisotropy in α -phase phosphorene through superlattice designYuanyuan He,^{1,2} Shiyun Xiong,^{1,*} Feifei Xia,¹ Zhibin Shao,¹ Jianwei Zhao,² Xiujuan Zhang,¹
Jiansheng Jie,^{1,†} and Xiaohong Zhang^{1,‡}¹*Institute of Functional Nano& Soft Materials (FUNSOM), Jiangsu Key Laboratory for Carbon-Based Functional Materials & Devices, Soochow University, Suzhou 215123, Jiangsu, People's Republic of China*²*College of Material and Textile Engineering, Jiaying University, Jiaying 314001, Zhejiang, People's Republic of China*

(Received 20 April 2017; revised manuscript received 21 December 2017; published 12 February 2018)

Rational tuning the anisotropic electronic properties of monolayer phosphorene is essential to their applications in electronic and optoelectronic devices. By combining the density functional theory and the nonequilibrium Green's function method, we developed a strategy to tune the anisotropic transport properties of phosphorene by designing stable arsenic-phosphorene ($\text{As}_x\text{P}_{1-x}$) superlattice (SL). It was found that, with a careful design of As:P ratio and atomic arrangement, the anisotropic transport properties could be tuned in a wide range. The transport current along the zigzag direction, which is very low in pristine phosphorene, was gradually enhanced by increasing the As:P ratio, and even became larger than that along armchair direction when the As:P ratio achieved 1:1 under a given arrangement of As atoms in $\text{As}_x\text{P}_{1-x}$ SL. The tunable anisotropic transport properties of $\text{As}_x\text{P}_{1-x}$ SL are attributed to the interplay between the different scattering rates related to the number and orientation of As-P interfaces. This finding demonstrates that the $\text{As}_x\text{P}_{1-x}$ SL design could be an effective approach to tune the anisotropic electronic properties of monolayer phosphorene, which is important for the development of high-performance electronic and optoelectronic devices based on phosphorene.

DOI: [10.1103/PhysRevB.97.085119](https://doi.org/10.1103/PhysRevB.97.085119)**I. INTRODUCTION**

In the past decade, two-dimensional (2D) semiconductors such as graphene, transition metal dichalcogenides (TMDs), and V-VI group topological insulators (TIs) have attracted tremendous attention due to their distinct structural, electronic, and optical properties. They have found important applications in new-generation devices, including field-effect transistors (FETs), memories, supercapacitors, and solar cells, etc. [1–6]. Among various 2D semiconductors, phosphorene displays extraordinary electronic and optoelectronic properties and has been intensively studied in recent years [7–11]. The direct band gap of phosphorene can be tuned in a wide range from 1.51 eV for monolayer to 0.59 eV for five-layer structure. It also possesses a high carrier mobility in the range of $10^3 - 10^4 \text{ cm}^2 \text{ V}^{-1} \text{ s}^{-1}$ at room temperature, almost equivalent to that of graphene ($10^4 \text{ cm}^2 \text{ V}^{-1} \text{ s}^{-1}$). The preparation of few-layer phosphorene through mechanical exfoliation technique has inspired extensive interest of its applications in high-performance nanodevices [12–14]. For instance, few-layer phosphorene has been utilized as the channel material in FETs, which exhibited outstanding device performance with large drain current modulation ratio up to $\sim 10^5$ and high field-effect mobility up to $\sim 10^3 \text{ cm}^2 \text{ V}^{-1} \text{ s}^{-1}$ [15,16].

It is well known that phosphorene shows strong anisotropic optical, mechanical, and electronic transport properties, owing to its puckered geometry [17]. Theoretical study indicates that, in monolayer phosphorene, the current flowing along

the armchair direction is about two orders of magnitude higher than that along the zigzag direction. However, it is also observed that electron mobility in armchair direction will decrease rapidly under strain effect, in contrast to the enhanced mobility in zigzag direction [18]. In common sense, strain is inevitable during the device fabrication and operation; thus it may cause the serious degradation of device performance if the device has a channel direction of armchair. Though the device with a zigzag channel will not suffer from the strain and, on the contrary, it could be a favorable factor, the low conductivity along this direction restricts the improvement of device performance. On the other hand, the strong anisotropic transport characteristics of phosphorene may greatly impact the reproducibility of the devices, since it is difficult to exactly determine the channel direction during device fabrication; the deviation of device channel from armchair/zigzag direction will cause a large device performance fluctuation. To overcome these drawbacks, one feasible route is to tune the anisotropic electronic transport properties of phosphorene, especially to improve the conductivity in the zigzag direction. To date, various methods, such as the introduction of vacancy defects and the substitutional doping, have been theoretically proven as effective methods to tune the anisotropic properties of phosphorene [19,20]. Nevertheless, the introduction of defects/doping atoms will inevitably break the periodic structure of phosphorene and introduce additional scattering centers in its lattice, leading to reduced conductivity and consequently degraded device performance.

The formation of arsenic-phosphorene ($\text{As}_x\text{P}_{1-x}$) superlattice (SL), the phase of which is the same as that of pristine phosphorene, has been proven an effective way to tune the optoelectronic properties [21,22]. Theoretical calculations based on density functional theory (DFT) have revealed that,

*xiongshiyun216@163.com

†jsjie@suda.edu.cn

‡xiaohong_zhang@suda.edu.cn

by changing the As atom percentage and its arrangement, there existed a structural transition from α to β phases and a transition from a direct band gap to an indirect one in $\text{As}_x\text{P}_{1-x}$ SL [22,23]. The 2D- $\text{As}_x\text{P}_{1-x}$ SL might be synthesized *via* chemical vapor transport method, which has been successfully applied to fabricate high-quality 2D monolayers with puckered honeycomb structure and SLs [24–28]. To prevent disordering of the SL monolayer caused by diffusion of intentionally doped As atoms during the growth and processing, low-diffusive atoms can be used for *n*- and *p*-type impurities [29]. Transmission x-ray measurements enable spatial mapping of the SL, such as grain size, orientation, uniformity, strain, and so on [30], which can further ensure the periodic arrangement of doped As atoms by means of characterization. SLs have been regarded as promising candidates to tune the transport properties of semiconductors. Previously, researchers have focused their effects on the phonon transport properties [31–33]. Nevertheless, the dynamic electronic transport behaviors in $\text{As}_x\text{P}_{1-x}$ SL, which are directly related to the optoelectronic device performance, have not been clarified yet. To promote the applications of phosphorene in high-performance devices, a detailed understanding on the anisotropic dynamic electronic transport behaviors of $\text{As}_x\text{P}_{1-x}$ monolayer is desirable.

Herein, by combining DFT and the nonequilibrium Green's function formalism (NEGF), we developed a superlattice designing strategy to tune the anisotropic electron transport properties of phosphorene. Through changing the atomic ratio and the arrangement of As atoms in $\text{As}_x\text{P}_{1-x}$ SL, the conduction current along zigzag direction could be remarkably enhanced, making it possible to reverse the preferable current flowing direction from armchair in pristine phosphorene to zigzag in $\text{As}_{0.5}\text{P}_{0.5}$ SL. Dynamic transmission study demonstrated that the incorporated As atoms allowed more efficient carrier transportation in $\text{As}_x\text{P}_{1-x}$; meanwhile, it weakened the π conjugation along the armchair direction, contributing to the reversal of preferable current flowing direction. Moreover, internal charge transfer on As-P covalent bonds was observed, which could effectively separate electrons and holes in $\text{As}_x\text{P}_{1-x}$ and lead to an increased carrier concentration. The superlattice designing strategy demonstrated in this work has shown its great potential in designing 2D semiconductor materials with superior electrical properties for high-performance devices.

II. METHODOLOGY

First-principle computations of monolayer $\text{As}_x\text{P}_{1-x}$ SLs with various chemical compositions and atomic arrangements were implemented in Atomistix Toolkit (ATK) software [34]. First, *ab initio* DFT was utilized to optimize the structures of monolayer $\text{As}_x\text{P}_{1-x}$ SLs and to calculate their static electronic properties. During geometry optimization, the generalized gradient approximation (GGA) with the Perdew-Burke-Ernzerhof (PBE) was adopted to describe the correction of the electronic exchange and correlation effects [35]. Norm-conserving Troullier-Martins pseudopotentials were used to approximate the interactions of the valence and core electrons [36]. A double- ζ plus polarization basis set (DZP) was employed to expand the wave functions. To avoid the interaction between adjacent layers, a large vacuum space ($= 20 \text{ \AA}$) was

set along the direction perpendicular to the sheet plane. A well-converged *k*-point grid of $5 \times 5 \times 1$ was adopted to sample the Brillouin zone of $\text{As}_x\text{P}_{1-x}$ SLs in the *x*, *y*, and *z* directions for structural optimization and static electronic property calculations. A cutoff energy of 600 Ry was kept to determine the self-consistent charge density to achieve a balance between calculation efficiency and accuracy. All geometries were fully optimized with the maximum atomic force and stress less than 10^{-2} eV/\AA and $5 \times 10^{-4} \text{ eV/\AA}$, respectively. The phonon spectrum calculation is obtained with finite displacement method implemented in CASTEP package [37]. A plane-wave energy cutoff of 500 eV with ultrasoft pseudopotential is used. To consider the effect of layer-layer interaction, DFT+D2 method with van der Waals force correction is employed to simulate the interlayer interaction of $\text{As}_x\text{P}_{1-x}$ SLs [38].

Subsequently, the electronic transport behaviors of $\text{As}_x\text{P}_{1-x}$ monolayers were examined by DFT combined with NEGF method. The central scattering region of $\text{As}_x\text{P}_{1-x}$ was sandwiched between semi-infinite source (left electrode) and drain (right electrode) regions. A 2×2 and a 2×9 supercell was chosen for the electrodes and the central scattering region, respectively. The size of the scattering region was tested to be long enough to damp out charge oscillations at the end layer under electric field. Such two-probe configuration was applied in the following calculations of *I-V* curves, transfer characteristic curves, transmission spectra, device density of states (DDOS), and so on. The Brillouin zone was represented by Monkhorst-Pack *k*-point mesh of $4 \times 1 \times 100$ for geometry optimization and for computation of dynamic electronic transport properties. All the atoms in the central scattering regions were relaxed until the force on each atom was less than 0.10 eV/\AA , while the atoms in the electrodes were fixed at their bulk positions.

III. RESULTS AND DISCUSSION

To study the change of lattice constants in monolayer $\text{As}_x\text{P}_{1-x}$ SLs, we gradually increase As concentration ($x = [\text{As}]/([\text{As}] + [\text{P}])$) from 0 to 1.0, in which $x = 0$ denotes the pristine phosphorene and $x = 1.0$ refers to the pristine arsenene. Figures 1(a)–1(e) display the structures of pristine phosphorene, $\text{As}_x\text{P}_{1-x}$ SLs, and arsenene, respectively. The monolayer geometry of each superlattice has been fully optimized. It is observed that the lattice constant increases gradually with increasing *x* due to the larger atomic radius of As atom (1.21 \AA) than P atom (1.06 \AA). Specifically, the lattice constants in the zigzag and armchair directions are enlarged by 13.0% and 11.6%, respectively, when *x* changes from 0 to 1.0. Also, the different sizes of As and P atoms in $\text{As}_x\text{P}_{1-x}$ ($0 < x < 1$) distort the uniform lattice of pristine phosphorene and arsenene. To further illustrate the influence of atomic arrangement on the lattice structures of $\text{As}_x\text{P}_{1-x}$ SLs, we have adjusted the relative positions of As and P atoms to form another allotrope of $\text{As}_{0.5}\text{P}_{0.5}$ SL, as shown in Fig. 1(f). The other two allotropes at $x = 0.5$ are also considered but the phonon dispersion calculation shows they are unstable due to the appearance of imaginary frequency. All the structures considered here are stable according to our phonon dispersion calculations (see Supplemental Material [39]), which also agrees with the previous reports [21,22]. The two allotropes

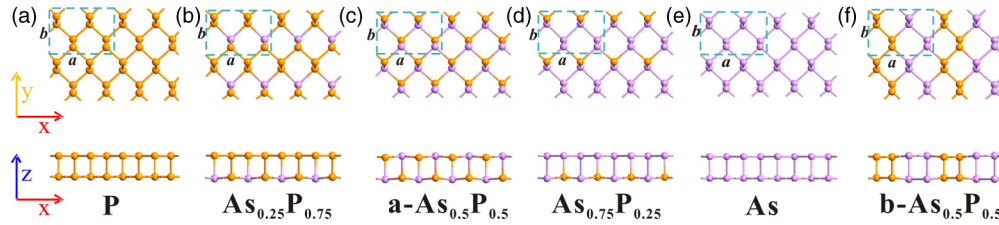


FIG. 1. Top and side views of equilibrium structures for monolayer (a) pristine phosphorene, (b) $\text{As}_{0.25}\text{P}_{0.75}$, (c) $\text{a-As}_{0.5}\text{P}_{0.5}$, (d) $\text{As}_{0.75}\text{P}_{0.25}$, (e) pristine arsenene, and (f) $\text{b-As}_{0.5}\text{P}_{0.5}$, respectively. The region in the cyan dashed frame is the unit cell, in which a and b are the lengths along the x and y directions, respectively.

of $\text{As}_{0.5}\text{P}_{0.5}$ show different bonding characteristics. For $\text{a-As}_{0.5}\text{P}_{0.5}$, the As-P bonds (interfaces) are perpendicular to the armchair direction, while the interfaces in $\text{b-As}_{0.5}\text{P}_{0.5}$ are perpendicular to the zigzag direction. The equilibrium structures discussed above indicate that both the atomic ratio and arrangement of incorporated As atoms can directly affect the bonding modes in monolayer $\text{As}_x\text{P}_{1-x}$ SLs. Note that in some of our designed SLs, the length of As or/and P component is smaller than one lattice period within one SL period; this type of SL can be called a fractional SL [40,41]. To simplify the notation, we still call it SLs. The considered SLs here may not be the most stable arrangements [22], but they can stably exist according to our phonon dispersion calculations. That means to transit to the most stable structure (phase separated or random alloyed structures), they will need to overcome an energy barrier.

To investigate the static electronic properties of $\text{As}_x\text{P}_{1-x}$ SLs, the difference charge densities ($\Delta\rho$) are shown in Fig. 2(a). $\Delta\rho$ is defined as $\Delta\rho = \rho_{\text{As}} - \rho_{\text{P}}$, where $\rho_{\text{As/P}}$ represents the total electrons gain/loss on all As/P atoms in the unit cell. $\rho_{\text{As/P}}$ is given by $\rho_{\text{As/P}} = N_{\text{As/P}}(5 - m_{\text{As/P}})$, where 5 is the valence electron number of the neutral As/P atom, N and $m_{\text{P/As}}$ are the number of As/P atoms in the unit cell, and the valence electron number of As/P atom in $\text{As}_x\text{P}_{1-x}$

SL, respectively. The regions of electron accumulation and depletion are displayed in blue and red, respectively. Note that the amount of electron accumulation on As and P atoms is different when $\text{As}_x\text{P}_{1-x}$ SLs are formed, owing to a small difference between the electronegativity of As and P atoms. The electron redistribution is more remarkable when the As concentration increases to $x = 0.5$, revealing a small amount of internal electron transfer from As to P atoms in $\text{As}_x\text{P}_{1-x}$ SL, which is quantitatively revealed by the Mulliken charge transfer [Fig. 2(b)] between As and P atoms (Δq) in a 2×9 $\text{As}_x\text{P}_{1-x}$ monolayer cell along the armchair and zigzag directions. The charge transfer between As and P atoms in $\text{As}_x\text{P}_{1-x}$ SL is strongly dependent on the number of As-P covalent bonds. In comparison to $\text{As}_x\text{P}_{1-x}$ SLs with other x values, $\text{a-As}_{0.5}\text{P}_{0.5}$ possesses the maximum number of As-P covalent bonds. Correspondingly, the charge transfer between As and P atoms in $\text{a-As}_{0.5}\text{P}_{0.5}$ is the strongest. Since the number of As-P covalent bonds also depends on the atomic arrangement, the charge transfer amount will vary in different allotropes. In $\text{a-As}_{0.5}\text{P}_{0.5}$, it contains much more As-P bonds than that in $\text{b-As}_{0.5}\text{P}_{0.5}$. By coincidence, the internal charge transfer in $\text{a-As}_{0.5}\text{P}_{0.5}$ is much larger than that in $\text{b-As}_{0.5}\text{P}_{0.5}$.

To gain insight into the effect of $\text{As}_x\text{P}_{1-x}$ SLs on the anisotropic electronic transport properties, we calculated the currents both along the armchair and zigzag directions for the two-probe $\text{As}_x\text{P}_{1-x}$ systems. Figure 3(a) shows the schematic illustrations for electronic transport calculations with NEGF. According to the Landauer-Büttiker formula, the current is written as [42]

$$I = \frac{2e}{h} \int_{-\infty}^{+\infty} \{T(E, V_b)[f(E - \mu_L) - f(E - \mu_R)]\} dE, \quad (1)$$

where f is the Fermi function, μ_L and μ_R are the electrochemical potentials of the left and right electrodes, respectively, and $T(E, V_b)$ is the transmission coefficient of charge carriers transmitting through the device at a given bias voltage with the energy E . The difference in the electrochemical potentials is given by eV with the applied bias voltage V , i.e., $\mu_L(V) = \mu_L(0) - eV/2$ and $\mu_R(V) = \mu_R(0) + eV/2$. For $\text{As}_x\text{P}_{1-x}$ along the zigzag direction, the current is significantly enhanced by the formation of $\text{As}_x\text{P}_{1-x}$ SL, as shown in Figs. 3(b)–3(f). In contrast, the current along the armchair direction is suppressed when the As concentration increases up to 0.5. Significantly, at the bias of 2.0 V, the current through the zigzag direction of $\text{a-As}_{0.5}\text{P}_{0.5}$ is enhanced by 27.9 times compared to that in the zigzag phosphorene. However, the current through the armchair direction is only 27.2% of that

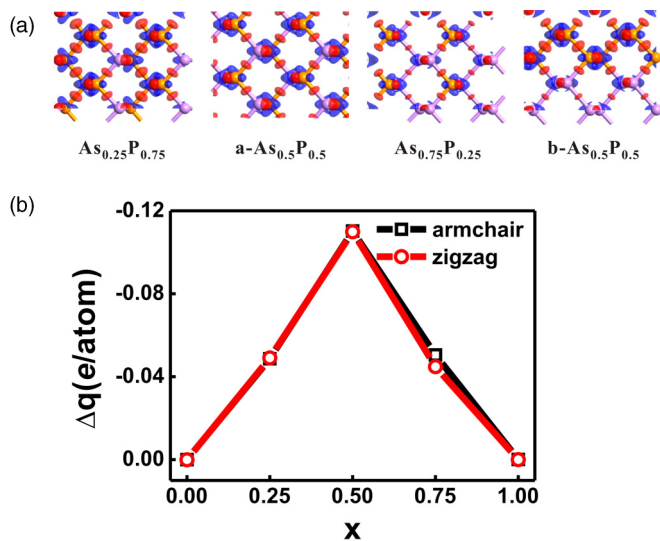


FIG. 2. (a) Difference charge densities ($e/\text{\AA}^3$) in $\text{As}_x\text{P}_{1-x}$ SLs as a function of As concentration x and arrangement, respectively. (b) Plots of Mulliken charge transfer amount between P and As atoms in $\text{As}_x\text{P}_{1-x}$ SLs as functions of As concentration.

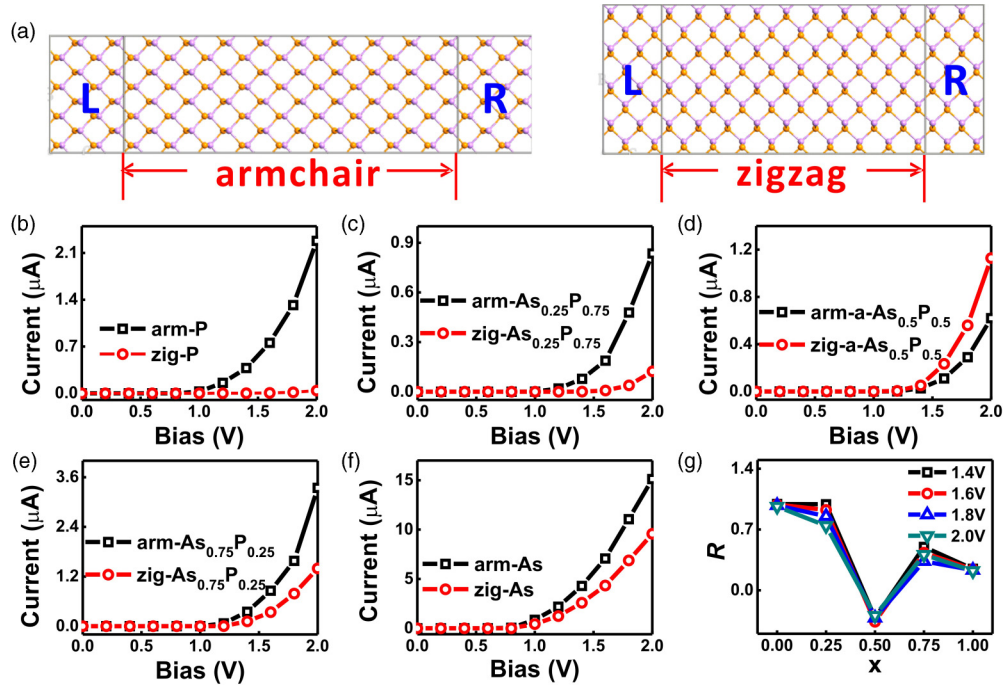


FIG. 3. (a) Schematic setup for transport calculations of $\text{As}_x\text{P}_{1-x}$ SLs along the armchair and zigzag directions, respectively. L and R represent the left and right electrodes. (b)–(f) Calculated anisotropic I - V curves for $\text{As}_x\text{P}_{1-x}$ with varied atomic ratios. (g) The anisotropic current ratio curves for $\text{As}_x\text{P}_{1-x}$ as a function of atomic ratio.

in armchair phosphorene. The above results demonstrate that designing $\text{As}_x\text{P}_{1-x}$ SL can effectively tune the anisotropic electrical transport of phosphorene.

Generally, the anisotropic transport behaviors of $\text{As}_x\text{P}_{1-x}$ SLs can be quantitatively characterized by the anisotropic current ratio between the zigzag and armchair directions: $R = (I_{\text{armchair}} - I_{\text{zigzag}})/(I_{\text{armchair}} + I_{\text{zigzag}})$, in which I_{armchair} and I_{zigzag} indicate the current along the armchair and zigzag directions, respectively. In this definition, the absolute value $\text{abs}(R) = 0$ and $\text{abs}(R) = 1$ corresponds to the extreme values of isotropic and anisotropic transport, respectively. While the sign of R indicates the relative magnitude between I_{armchair} and I_{zigzag} . Figure 3(g) shows the calculated anisotropic current ratio curves for $\text{As}_x\text{P}_{1-x}$ SLs at the bias above 1.2 V. The pristine phosphorene displays a strong anisotropic transport behavior with $R > 0$ (1.00 at the bias of 1.4 V), indicating a much better armchair conductance. In $\text{As}_x\text{P}_{1-x}$ SLs, valence electrons can move more freely around As nucleus than around P nucleus due to the larger atomic radius of As atom. The increase of As atomic ratio can enhance the overall mobility of the superlattice systems. In the meantime, the incorporation of As atoms into phosphorene monolayer will introduce As-P interfaces, which will reduce the conduction due to the carrier scattering. Therefore, the resulted current of $\text{As}_x\text{P}_{1-x}$ SL is the interplay between the higher freedom of valence electrons around As nucleus and the scattering at As-P interfaces. Because the As-P interface is perpendicular to the armchair direction in $\text{As}_{0.25}\text{P}_{0.75}$, a- $\text{As}_{0.5}\text{P}_{0.5}$, and $\text{As}_{0.75}\text{P}_{0.25}$ superlattices, the current along the armchair direction tends to decrease when the As:P ratio approaches 1:1, i.e., x approaches 0.5, due to the stronger scattering effect, while, in the zigzag direction, the scattering is much weaker as the current flow is

parallel to the As-P interfaces in a- $\text{As}_{0.5}\text{P}_{0.5}$ and $\text{As}_{0.75}\text{P}_{0.25}$ monolayers. As a result, the higher freedom of valence electrons predominates the current strength, leading to an enhanced current with increasing As concentration. The two different behaviors of the current in the zigzag and armchair directions eventually tune the anisotropic ratio from $R > 0$ in pristine phosphorene and arsenene to $R < 0$ (-0.32 at the bias of 1.4 V) in a- $\text{As}_{0.5}\text{P}_{0.5}$ SL, i.e., a reversed anisotropic transport behavior.

The atomic arrangement can also influence the anisotropic transport behaviors of $\text{As}_x\text{P}_{1-x}$ SLs. In the two allotropes of $\text{As}_{0.5}\text{P}_{0.5}$ SL, the current shows different preferable flowing directions (see Supplemental Material [39] for the calculated anisotropic I - V curves for $\text{As}_x\text{P}_{1-x}$ with varied atomic arrangements). In a- $\text{As}_{0.5}\text{P}_{0.5}$ systems, the As-P interface is perpendicular to the armchair direction, which results in a strong carrier scattering in this direction and thus suppresses the armchair current. However, opposite to a- $\text{As}_{0.5}\text{P}_{0.5}$ allotrope, the preferable current flowing in b- $\text{As}_{0.5}\text{P}_{0.5}$ is along the armchair direction with $R > 0$ value (0.97 at the bias of 1.4 V). The reason for this observation is that the As-P interface in b- $\text{As}_{0.5}\text{P}_{0.5}$ is perpendicular to the zigzag direction, which brings severe carrier scattering in this direction. Therefore, the electronic transport anisotropy of $\text{As}_x\text{P}_{1-x}$ monolayer can also be reversed by changing the atomic arrangement.

For the pristine phosphorene and arsenene, it is known that the lattice strain can reduce the electron mobility along the armchair direction, in contrast to the increase of electron mobility in zigzag direction [18,43]. Although arsenene monolayer has the best electron transport properties in both armchair and zigzag directions among all the studied structures, its device performance may be degraded since strain is inevitable in

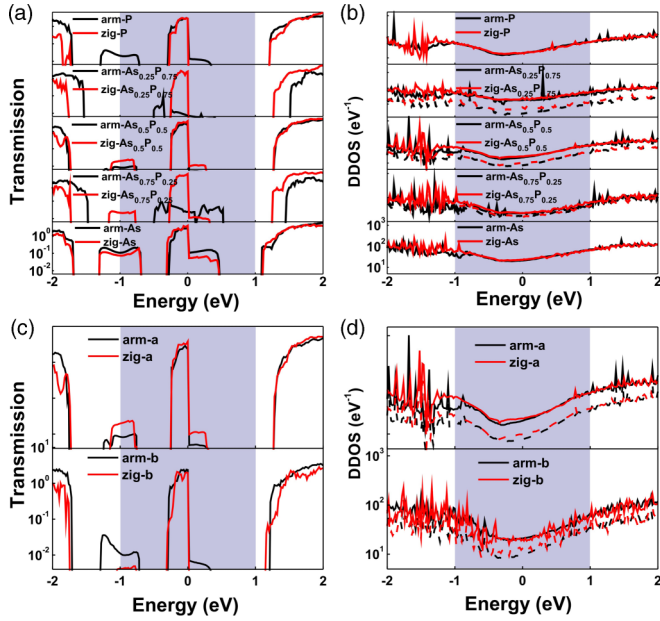


FIG. 4. (a) Transmission and (b) DDOS spectra of As_xP_{1-x} SLs with various atomic ratios at 2.0 V. (c) Transmission and (d) DDOS spectra of the two allotropes of $As_{0.5}P_{0.5}$ at 2.0 V. The shadow regions denote the bias windows. The Fermi level of electrodes is set to be 0 eV. The dash curves in DDOS spectra represent the partial DOS localized on As atoms.

devices. Besides, it was found that the helical angle alignment is essential to achieve the optimum performance of pure phosphorene-based devices or electrical circuits due to its large anisotropy [44]. The optimization and reproduction of device performances, however, remains a big challenge due to the uncontrollability of monolayer orientation in devices. In pure arsenene, the reduced electron mobility by strain in the armchair direction will enhance its anisotropy. Consequently, the device properties will also be hard to optimize and reproduce. By contrast, the above drawbacks can be overcome to a large extent by the formation of stable As_xP_{1-x} SLs. The armchair and zigzag directional I - V curves in the Supplemental Material [39] indicate that the existence of strain in $a-As_{0.5}P_{0.5}$ monolayer can significantly improve the conductance along both the armchair and zigzag directions. As a result, the device performance could be largely improved under strain. In fact, the improved conductivity of As_xP_{1-x} SLs under stress is very promising for their applications in flexible electronic devices [45,46]. Moreover, in As_xP_{1-x} SLs, the anisotropy can be tuned with the change of As:P ratio and As atomic arrangement. Consequently, one can minimize the anisotropy of As_xP_{1-x} SLs and largely improve the reproducibility of device properties.

The anisotropic transport characteristics of As_xP_{1-x} SLs can be further understood by the transmission spectra and the device density of states (DDOS). Figure 4(a) plots the transmission coefficient $T(E, V)$ versus the energy E for As_xP_{1-x} SLs at the bias of 2.0 V, in which x ranges from 0, 0.25, 0.50, 0.75 to 1.00. Here the Fermi level of the electrode is set to $E_F = 0$. Generally, the applied bias will create offsets of band structures in different regions along the transport direction,

thus decreasing the energy difference between the valence band maximum (VBM) of the source electrode and the conduction band minimum (CBM) of the drain electrode [19]. As the applied bias is larger than the band gaps of the electrodes, some conduction channels are created in the region around Fermi level due to the overlapping of the source electrode-valence band and the drain electrode-conduction band. The transmission spectrum, which determines the current according to the Landauer-Büttiker theory [47], is dependent on the alignment of the states of electrode and scattering regions. The first transmission peaks below and above the Fermi level are initiated by the VBM and the CBM, respectively. Since the VBM peaks in all As_xP_{1-x} systems are close to the Fermi level and much stronger than the CBM peaks, the currents are mostly contributed by the VBM resonance, indicating a p -type conduction of As_xP_{1-x} monolayers.

Based on the transmission spectra, it is seen that, for the pristine phosphorene, the number of transmission peaks and the amplitude of the peaks along the armchair direction are much larger than those along the zigzag direction, thus leading to an anisotropic transport with $R > 0$. However, in the armchair As_xP_{1-x} systems, the transmission coefficient of the VBM peak first decreases with the increase of x , from 3.00 (pristine phosphorene) to 0.93 ($As_{0.25}P_{0.75}$), and then increases gradually to 3.85 (pristine arsenene). The reduction of transmission coefficient in As_xP_{1-x} along the armchair direction can be ascribed to the strong interface scattering, because the As-P interface is perpendicular to the armchair direction. In contrast, the transmission of zigzag- As_xP_{1-x} monolayers shows an opposite tendency with the increase of x . The main feature is the appearance of two new transmission peaks when the As concentration is larger than 0.5, i.e., the peak around the left edge of the bias window and the one above the Fermi level. Both the width and the height of the two peaks are enhanced with x increase. In As_xP_{1-x} SLs, the weakened interface scattering in zigzag direction promotes the electron transmission, because the As-P interfaces are parallel to the zigzag direction. Also, the higher freedom of valence electrons around the As nucleus contributes to the enhanced transmission along the zigzag direction. The opposite tendency of transmission along the armchair direction and along the zigzag direction with the incorporation of As atoms into the phosphorene lattice gradually tunes the anisotropic transport properties of phosphorene and eventually results in a reversed current conduction in $a-As_{0.5}P_{0.5}$. Moreover, the contribution from As atoms to the total transport probabilities of monolayer As_xP_{1-x} could be reflected by the DDOS, as shown in Fig. 4(b). The DOS projected on As atoms increases with x value. As a result, the current along the zigzag direction is enhanced by almost 240 times from $0.04 \mu A$ for pristine phosphorene to $1.13 \mu A$ for $a-As_{0.5}P_{0.5}$. Therefore, if the number of As-P interfaces is fixed, a higher atomic ratio of As atoms in As_xP_{1-x} SLs is a favorable factor that can promote the electronic transport efficiency.

In addition to the atomic ratio, impact of atomic arrangement of As atoms on the electronic transport anisotropy of As_xP_{1-x} monolayers was further evaluated. Figures 4(c) and 4(d) display the transmission spectra and DDOS of the two $As_{0.5}P_{0.5}$ allotropes at 2.0 V, respectively. Due to a different interface orientation, the transmission along the zigzag direction within the bias window is suppressed when the allotrope

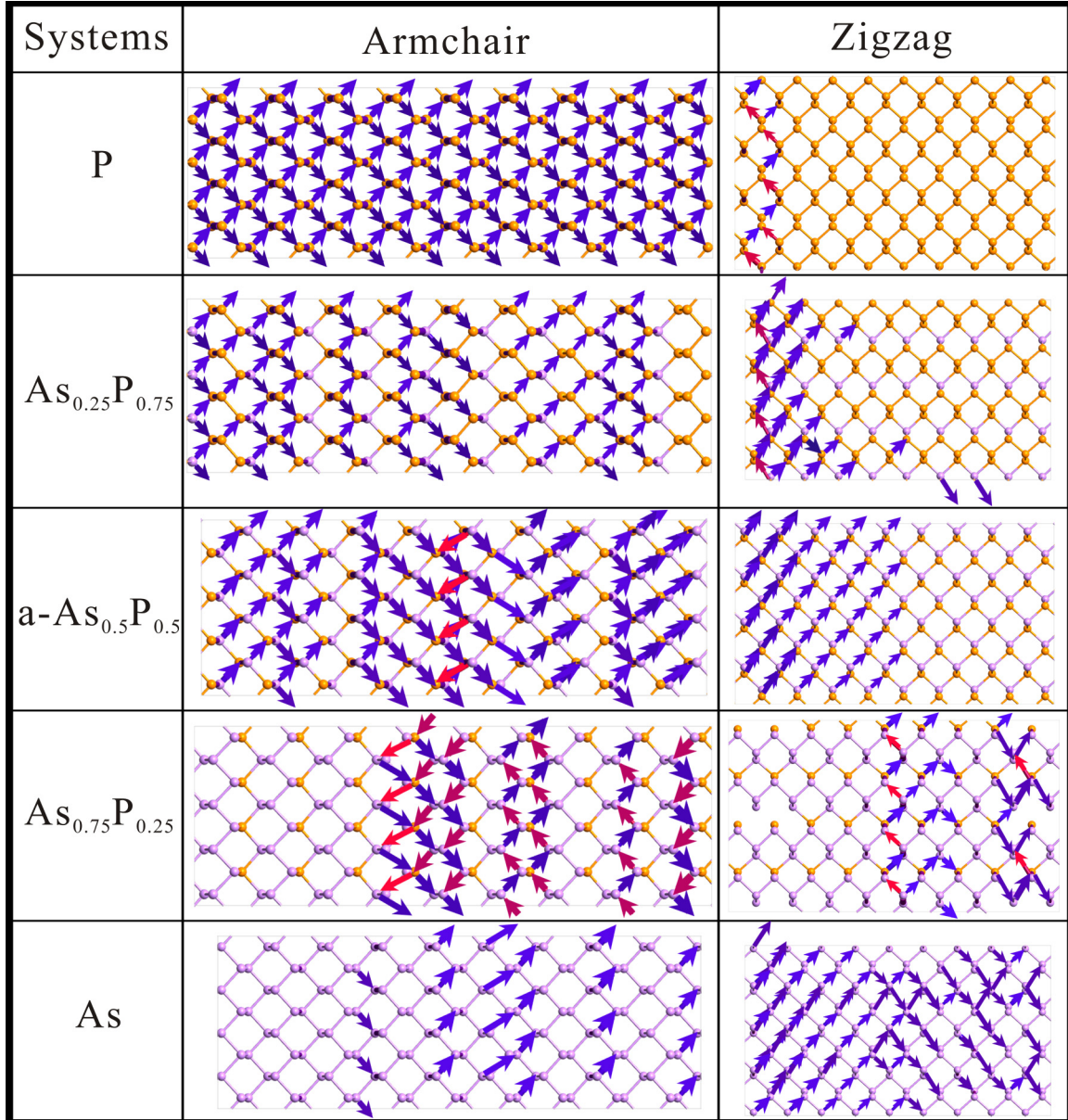


FIG. 5. Local transmissions through $\text{As}_x\text{P}_{1-x}$ monolayers with different atomic ratios at the energy level of 0.20 eV under the bias of 2.0 V. The Fermi level of $\text{As}_x\text{P}_{1-x}$ electrodes is set to be 0 eV.

of $\text{As}_{0.5}\text{P}_{0.5}$ changes from a-type to b-type. In contrast, because the interface is perpendicular to the zigzag direction in b- $\text{As}_{0.5}\text{P}_{0.5}$, the transmission in the armchair direction is stronger than that in the zigzag direction.

To check how the As:P ratio affects the transmission channel at the atomic scale, we have analyzed the local transmission function with the variation of As concentration (Fig. 5). The local transmission function can provide a striking picture on how carriers are transported through the atomic bonds [47,48]. In this method, the transmission can be decomposed into local (atomic) contributions as follows:

$$T(E) = \sum_{A \in L, B \in R} T_{AB}(E), \quad (2)$$

where T_{AB} is the transmission between the atoms A and B . T_{AB} can be calculated on the basis of the Fock and overlap matrices that are the same as those used for the transmission calculation.

Local transmission plots in Fig. 5 illustrate how the local transmission pattern is changed with x . The local transmission plots are normalized by the maximum value in each plot. The transmission probability of each channel is illustrated by the arrow diameter. To clearly illustrate the figure, we have set a threshold of 0.4, below which the arrows are not shown. The blue arrows indicate the components of the transmission that is in the direction of net current flow, thereby contributing to the current, whereas the red arrows give components in the opposite direction, thereby reducing the net current, and the purple arrows give components in the perpendicular direction, thereby scattering the carriers. The local transmission in the pristine phosphorene demonstrates that the main transmission

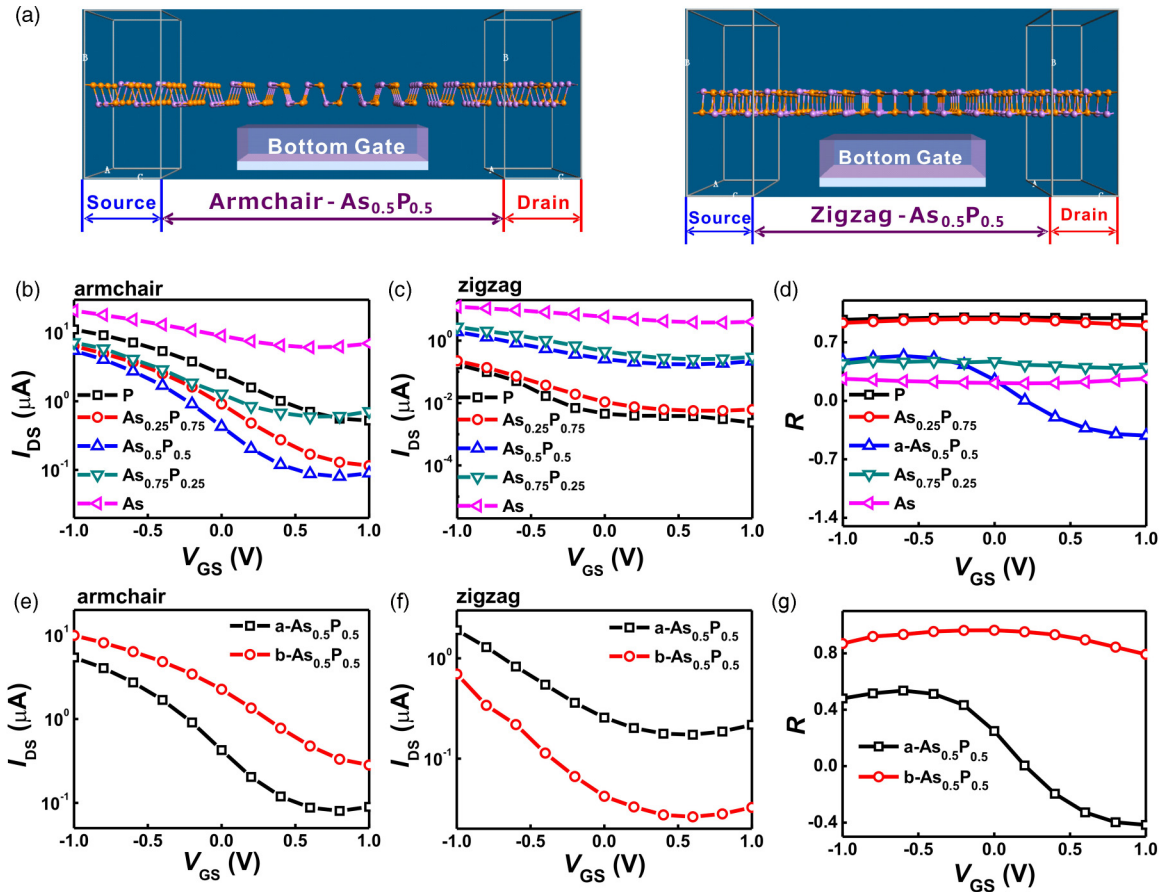


FIG. 6. (a) Schematic setups of the bottom-gate FET devices based on $\text{As}_x\text{P}_{1-x}$ monolayers along the armchair and zigzag directions, respectively. Anisotropic transfer characteristic curves of monolayer $\text{As}_x\text{P}_{1-x}$ FETs with varied atomic ratios (b), (c) and allotropes of $\text{As}_{0.5}\text{P}_{0.5}$ FETs with various atomic arrangements (d), (e) at $V_{DS} = 1.6$ V. The anisotropic current ratio curves for $\text{As}_x\text{P}_{1-x}$ with varied atomic ratios (f) and atomic arrangements (g) as a function of V_{GS} ranging from -1.0 to 1.0 V.

is through the π -conjugated P-P bonds. The orientation of P-P covalent bonds is accordant with the direction of the net current in the armchair phosphorene, thus leading to a large electrical current. However, their orientation is almost perpendicular to the net current in the zigzag phosphorene, which hinders electrons to move between electrodes. This conjugated P-P bond alignment finally results in much different transport properties in the zigzag and armchair directions. The local transmission in the pristine arsenene also shows similar anisotropic transport behavior. In contrast, in $a\text{-As}_{0.5}\text{P}_{0.5}$ along the armchair direction, electrons are transmitted through the As-P covalent bonds with weakened π conjugation, i.e., the As-P interfaces. Although the transmission probabilities are large, there are transmissions in the opposite directions and in the directions perpendicular to the net current. This complicated transmission behavior indicates a strong scattering effect, which agrees well with the total transmission analysis. Hence the electron transport efficiency along the armchair direction is reduced and consequently the conduction current is suppressed. However, in the zigzag direction of $a\text{-As}_{0.5}\text{P}_{0.5}$, the transmission is predominated by the ones along the transport direction, indicating a minimized scattering effect and thus a large conduction current. As a result, the $a\text{-As}_{0.5}\text{P}_{0.5}$ system shows an opposite anisotropic transport property relative to the

pristine phosphorene/arsene. The local transmission in other $\text{As}_x\text{P}_{1-x}$ SLs with other As:P ratio varies between the above two cases: the pristine phosphorene/arsene and $a\text{-As}_{0.5}\text{P}_{0.5}$. Moreover, similar phenomena can also be observed from the spatial distribution of local density of states (LDOS), as shown in the Supplemental Material [39].

FET devices were constructed to directly assess the electrical characteristics of $\text{As}_x\text{P}_{1-x}$ SLs. Schematic setups of bottom-gate FETs based on $\text{As}_x\text{P}_{1-x}$ monolayers are illustrated in Fig. 6(a). The intrinsic channel materials consist of $a\text{-As}_{0.5}\text{P}_{0.5}$ monolayers along the armchair and zigzag directions, respectively, with the two ends in contact with the source and drain electrodes. The simulated regions are embedded on an HfO_2 ($k = 29\epsilon_0$) dielectric layer of 4.0 \AA in thickness. Metallic gate electrodes with a thickness of 1.0 \AA are attached to the dielectrics below the intrinsic channels. This kind of bottom-gate geometry provides highly gate-controlled electrical performance.

Figures 6(b) and 6(c) show the calculated transfer characteristic curves of $\text{As}_x\text{P}_{1-x}$ FETs with varied atomic ratios at a source-drain voltage (V_{DS}) of 1.6 V. The source-drain currents (I_{DS}) of $\text{As}_x\text{P}_{1-x}$ FETs decrease exponentially with increasing gate voltage (V_{GS}), indicating the p -type conduction characteristics of $\text{As}_x\text{P}_{1-x}$ semiconductors. In the armchair- $\text{As}_x\text{P}_{1-x}$

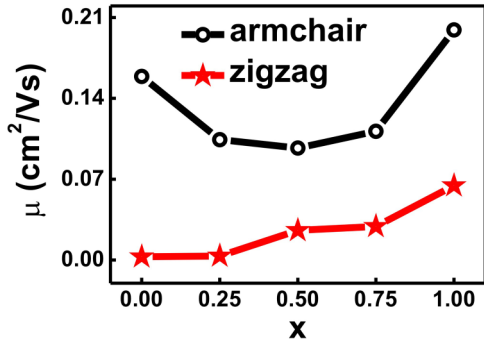


FIG. 7. Plots of anisotropic carrier mobility of $\text{As}_x\text{P}_{1-x}$ SLs as a function of atomic ratio.

based FETs, the formation of $\text{As}_x\text{P}_{1-x}$ SL results in a decreased I_{DS} , owing to the weakened π -coupling degree on As-P bonds that hinders electrons to transport through the armchair direction. In the case of the zigzag- $\text{As}_x\text{P}_{1-x}$ -based FETs, I_{DS} increases with x , which is due to the injection of carriers by the charge transfer between As and P atoms as well as the enhanced carrier mobility on As atoms. In the zigzag- $\text{As}_x\text{P}_{1-x}$ FETs, these positive factors predominate the electronic transport. However, in the armchair- $\text{As}_x\text{P}_{1-x}$ devices, the negative effect by carrier scattering at As-P interfaces is predominated. For instance, I_{DS} of the zigzag- $\text{As}_{0.75}\text{P}_{0.25}$ FET has been enhanced to $2.75 \mu\text{A}$ at $V_{\text{GS}} = -1.0 \text{ V}$, which is nearly 16 times that in the zigzag-phosphorene FET. In contrast, I_{DS} of the armchair- $\text{As}_{0.75}\text{P}_{0.25}$ FET is reduced to $7.18 \mu\text{A}$, corresponding to 64.8% of that in the armchair-phosphorene FET. Thereupon, the anisotropic device performance of phosphorene FET can be rationally modulated by changing the atomic ratio through designing $\text{As}_x\text{P}_{1-x}$ SLs.

Figures 6(e) and 6(f) depict the transfer characteristic curves of a- $\text{As}_{0.5}\text{P}_{0.5}$ and b- $\text{As}_{0.5}\text{P}_{0.5}$ FETs. In the armchair- $\text{As}_{0.5}\text{P}_{0.5}$ FETs, in accordance with the transmission analysis, b- $\text{As}_{0.5}\text{P}_{0.5}$ has higher I_{DS} value of $9.94 \mu\text{A}$ at $V_{\text{GS}} = -1.0 \text{ V}$, due to the minimized scattering effect at As-P interfaces, which are parallel to the transport direction. However, in the zigzag- $\text{As}_{0.5}\text{P}_{0.5}$ FETs, a- $\text{As}_{0.5}\text{P}_{0.5}$ shows a higher I_{DS} value of $1.91 \mu\text{A}$ at $V_{\text{GS}} = -1.0 \text{ V}$. The above results collectively demonstrate that the carrier scattering at As-P interface has a great impact on the electronic transport efficiency along the armchair direction.

The anisotropic device performances of $\text{As}_x\text{P}_{1-x}$ -FETs varied V_{GS} are further characterized in Figs. 6(d) and 6(g). From Fig. 6(d), it is seen that the anisotropic ratio, R value of a- $\text{As}_{0.5}\text{P}_{0.5}$ can be tuned from 0.48 to -0.42 , when V_{GS} changes from -1.0 V to 1.0 V , due to variation of the vertical electric field. However, for $\text{As}_x\text{P}_{1-x}$ with other x value, R values remain stable. Compared to a- $\text{As}_{0.5}\text{P}_{0.5}$, R value of b- $\text{As}_{0.5}\text{P}_{0.5}$ changes from 0.87 to 0.79 [Fig. 6(g)], showing a stable anisotropic device performance. Therefore, the V_{GS} -dependent R tendency of a- $\text{As}_{0.5}\text{P}_{0.5}$ FET reflects that controlling vertical electric field could offer another effective route to tune the anisotropic transport properties of $\text{As}_x\text{P}_{1-x}$ SLs, in addition to the atomic ratios and atomic arrangements.

Figure 7 plots the anisotropic carrier mobilities of $\text{As}_x\text{P}_{1-x}$ SLs with different As atomic ratios. Due to the use of angstrom-

scaled small devices, the simulated carrier mobilities are underestimated in general. In addition, since the width of armchair- $\text{As}_x\text{P}_{1-x}$ is narrower than that of zigzag- $\text{As}_x\text{P}_{1-x}$ with the same periodicity, while the length of armchair- $\text{As}_x\text{P}_{1-x}$ is larger than that of zigzag- $\text{As}_x\text{P}_{1-x}$ with the same periodicity, the calculated carrier mobility along the armchair direction is usually larger than that along zigzag direction [49]. However, the obtained results can still be used to predict the changing trends of carrier mobility in $\text{As}_x\text{P}_{1-x}$ monolayers with different atomic ratios and arrangements. It can be found that the carrier mobility along zigzag direction monotonously increases with the atomic ratio of As atoms in superlattices, whereas the mobility along the armchair direction first declines and then increases [Fig. 7(a)]. In the zigzag- $\text{As}_x\text{P}_{1-x}$ monolayers, the formation of $\text{As}_x\text{P}_{1-x}$ SL can provide additional valence orbitals, on which electrons can transport with higher mobility through the zigzag direction. Also, because the As-P interfaces are parallel to the direction of net current, the carrier scattering along the zigzag direction is much weaker. As a result, the less bounded electrons provided by As atoms predominate the overall mobility, leading to an enhanced mobility with the increase of As concentration. However, in the armchair- $\text{As}_x\text{P}_{1-x}$ monolayers, the positive factor of As atoms incorporation has been partly offset by the carrier scattering at As-P interfaces. Since the As-P interface density reaches maximum at $x = 0.5$, the overall mobility reaches a minimum value and then gradually enhances when x deviates from 0.5. On the other hand, for the two allotropes of $\text{As}_{0.5}\text{P}_{0.5}$, the mobility of b- $\text{As}_{0.5}\text{P}_{0.5}$ shows a larger difference between the armchair and zigzag directions, which is again due to the change of As-P interface orientation. In a- $\text{As}_{0.5}\text{P}_{0.5}$ superlattices, the As-P interface is perpendicular to the armchair direction, which results in a strong carrier scattering in this direction and thus suppresses the mobilities along the armchair direction. In contrast, in b- $\text{As}_{0.5}\text{P}_{0.5}$, the As-P interface is perpendicular to the zigzag direction, which suffers severe mobility reduction in this direction.

IV. CONCLUSION

In conclusion, by combining DFT with the NEGF method, we have theoretically developed a superlattice designing strategy to form $\text{As}_x\text{P}_{1-x}$ monolayers with tunable anisotropic transport properties. The incorporated As atoms provide valence orbitals for electrons to transport through $\text{As}_x\text{P}_{1-x}$ with higher mobility, due to their larger atomic radius than P atoms. The formation of As-P covalent bonds also initiates a small amount of internal charge transfer between As and P atoms. Nevertheless, the existence of As-P interfaces leads to carrier scattering from the direction of net current flow and the scattering strength strongly depends on the channel direction (armchair or zigzag). Under the interplay of the above factors, the anisotropic transport properties of $\text{As}_x\text{P}_{1-x}$ SLs can be efficiently reversed, by controlling the As:P ratio as well as atomic arrangement. Significantly, the anisotropic current ratio R between the armchair and zigzag directions has been remarkably tuned from 1.00 in pristine phosphorene to -0.32 in stable a- $\text{As}_{0.5}\text{P}_{0.5}$ at the bias of 1.4 V . This work sheds light on the potential application of superlattice designing in controlling the anisotropic electrical properties

of 2D semiconductors represented by phosphorene, which is of significance for their device conduction and performance improvement.

ACKNOWLEDGMENTS

This work was supported by the National Basic Research Program of China (Grant No. 2013CB933500), the Natural Science Foundation of Jiangsu Province (Grant

No. BK20160308), the National Natural Science Foundation of China (Grants No. 51172151, No. 21121091, and No. 21273113), Qing Lan Project, and a Project Funded by the Priority Academic Program Development of Jiangsu Higher Education Institutions (PAPD). We acknowledge the support from Collaborative Innovation Center of Suzhou Nano Science and Technology (NANO-CIC), and the computing resources and technical support from National Super Computing Center in Shenzhen (Shenzhen Cloud Computing Center).

-
- [1] J. Son, S. Lee, S. J. Kim, B. C. Park, H. K. Lee, S. Kim, J. H. Kim, B. H. Hong, and J. Hong, *Nat. Commun.* **7**, 13261 (2016).
- [2] M. V. Zhao, Y. Ye, Y. M. Han, Y. Xia, H. Y. Zhu, S. Q. Wang, Y. Wang, D. A. Muller, and X. Zhang, *Nat. Nanotechnol.* **11**, 954 (2016).
- [3] J. Wu, S. L. Feng, X. Z. Wei, J. Shen, W. Q. Lu, H. F. Shi, K. Tao, S. R. Lu, T. Sun, L. Y. Yu, C. L. Du, J. M. Miao, and L. K. Norford, *Adv. Funct. Mater.* **26**, 7462 (2016).
- [4] J. Shim, H. S. Kim, Y. S. Shim, D. H. Kang, H. Y. Park, J. Lee, J. Jeon, S. J. Jung, Y. J. Song, W. S. Jung, J. Lee, S. Park, J. Kim, S. Lee, Y. H. Kim, and J. H. Park, *Adv. Mater.* **28**, 5293 (2016).
- [5] N. Choudhary, C. Li, H.-S. Chung, J. Moore, J. Thomas, and Y. Jung, *ACS Nano* **10**, 10726 (2016).
- [6] J. S. Ponraj, Z. Q. Xu, S. C. Dhanabalan, H. R. Mu, Y. S. Wang, J. Yuan, P. F. Li, S. Thakur, M. Ashrafi, K. Mccoubrey, Y. P. Zhang, S. J. Li, H. Zhang, and Q. L. Bao, *Nanotechnology* **27**, 462001 (2016).
- [7] J. Q. He, D. W. He, Y. S. Wang, Q. N. Cui, M. Z. Bellus, H. Y. Chiu, and H. Zhao, *ACS Nano* **9**, 6436 (2015).
- [8] X. M. Wang, A. M. Jones, K. L. Seyler, V. Tran, Y. C. Jia, H. Zhao, H. Wang, L. Yang, X. D. Xu, and F. N. Xia, *Nat. Nanotechnol.* **10**, 517 (2015).
- [9] S. Balendhran, S. Walia, H. Nili, S. Sriram, and M. Bhaskaran, *Small* **11**, 640 (2015).
- [10] R. A. Doganov, E. C. T. O'Farrell, S. P. Koenig, Y. T. Yeo, A. Ziletti, A. Carvalho, D. K. Campbell, D. F. Coker, K. Watanabe, T. Taniguchi, A. H. C. Neto, and B. Ozyilmaz, *Nat. Commun.* **6**, 6647 (2015).
- [11] L. Z. Kou, C. F. Chen, and S. C. Smith, *J. Phys. Chem. Lett.* **6**, 2794 (2015).
- [12] S. P. Koenig, R. A. Doganov, H. Schmidt, A. H. C. Neto, and B. Ozyilmaz, *Appl. Phys. Lett.* **104**, 103106 (2014).
- [13] X. M. Ma, W. L. Lu, B. Y. Chen, D. L. Zhong, L. Huang, L. J. Dong, C. H. Jin, and Z. Y. Zhang, *AIP Adv.* **5**, 107112 (2015).
- [14] J. S. Miao, S. M. Zhang, L. Cai, M. Scherr, and C. Wang, *ACS Nano* **9**, 9236 (2015).
- [15] H. Liu, A. T. Neal, Z. Zhu, Z. Luo, X. F. Xu, D. Tomanek, and P. D. Ye, *ACS Nano* **8**, 4033 (2014).
- [16] L. K. Li, Y. J. Yu, G. J. Ye, Q. Q. Ge, X. D. Ou, H. Wu, D. L. Feng, X. H. Chen, and Y. B. Zhang, *Nat. Nanotechnol.* **9**, 372 (2014).
- [17] X. Ling, H. Wang, S. X. Huang, and F. N. Xia, *Proc. Natl. Acad. Sci. U.S.A.* **112**, 4523 (2015).
- [18] R. X. Fei and L. Yang, *Nano Lett.* **14**, 2884 (2014).
- [19] M. U. Farooq, A. Hashmi, and J. S. Hong, *Sci. Rep.* **5**, 12482 (2015).
- [20] C. X. Guo, C. X. Xia, L. Z. Fang, T. X. Wang, and Y. F. Liu, *Phys. Chem. Chem. Phys.* **18**, 25869 (2016).
- [21] M. Q. Xie, S. L. Zhang, B. Cai, Y. Huang, Y. S. Zou, B. Guo, Y. Gu, and H. B. Zeng, *Nano Energy* **28**, 433 (2016).
- [22] Z. Zhu, J. Guan, and D. Tomanek, *Nano Lett.* **15**, 6042 (2015).
- [23] F. Shojaei and H. S. Kang, *J. Phys. Chem. C* **119**, 20210 (2015).
- [24] D. K. Hu, G. C. Xu, L. Xing, X. X. Yan, J. Y. Wang, J. Y. Zheng, Z. X. Lu, P. Wang, X. Q. Pan, and L. Y. Jiao, *Angew. Chem. Int. Ed.* **56**, 3611 (2017).
- [25] B. L. Liu, M. Kopf, A. N. Abbas, X. M. Wang, Q. S. Guo, Y. C. Jia, F. N. Xia, R. Wehrich, F. Bachhuber, F. Pielhofer, H. Wang, R. Dhall, S. B. Cronin, M. Y. Ge, X. Fang, T. Nilges, and C. W. Zhou, *Adv. Mater.* **27**, 4423 (2015).
- [26] Q. H. Yang, L. R. Lou, and G. Wang, *Physica E* **89**, 124 (2017).
- [27] W. J. Qi, J. L. Zhang, C. L. Mo, X. L. Wang, X. M. Wu, Z. J. Quan, G. X. Wang, S. Pan, F. Fang, and J. L. Liu, *J. Appl. Phys.* **122**, 084504 (2017).
- [28] F. S. Chen, H. Chen, Z. Deng, T. P. Lu, Y. T. Fang, Y. Jiang, Z. G. Ma, and M. He, *Appl. Phys. A: Mater. Sci. Process.* **118**, 1453 (2015).
- [29] H. Saito, K. Uwai, and N. Kobayashi, *Jpn. J. Appl. Phys.* **32**, 10 (1993).
- [30] B. T. Diroll, V. V. T. Doan-Nguyen, M. Cargnello, E. A. Gaulding, C. R. Kagan, and C. B. Murray, *ACS Nano* **8**, 12843 (2014).
- [31] D. G. Cahill, P. V. Braun, G. Chen, D. R. Clarke, S. H. Fan, K. E. Goodson, P. Keblinski, W. P. King, G. D. Mahan, A. Majumdar, H. J. Maris, S. R. Phillpot, E. Pop, and L. Shi, *Appl. Phys. Rev.* **1**, 011305 (2014).
- [32] Y. K. Koh, Y. Cao, D. G. Cahill, and D. Jena, *Adv. Funct. Mater.* **19**, 610 (2009).
- [33] S. Y. Xiong, B. Latour, Y. X. Ni, S. Volz, and Y. Chalopin, *Phys. Rev. B* **91**, 224307 (2015).
- [34] Atomistix ToolKit by QuantumWise A/S, <http://www.quantumwise.com>.
- [35] J. P. Perdew, K. Burke, and M. Ernzerhof, *Phys. Rev. Lett.* **77**, 3865 (1996).
- [36] N. Troullier and J. L. Martins, *Phys. Rev. B* **43**, 1993 (1991).
- [37] S. J. Clark, M. D. Segall, C. J. Pickard, P. J. Hasnip, M. I. J. Probert, K. Refson, and M. C. Z. Payne, *Kristallogr.* **220**, 567 (2005).
- [38] S. J. Grimme, *Comput. Chem.* **27**, 1787 (2006).
- [39] See Supplemental Material at <http://link.aps.org/supplemental/10.1103/PhysRevB.97.085119> for detailed information about designed $\text{As}_x\text{P}_{1-x}$ fractional SLs, phonon band dispersions,

- anisotropic I - V curves with various atomic arrangements, arm-chair and zigzag directional I - V curves for a- $\text{As}_{0.5}\text{P}_{0.5}$ monolayer under the 5% stress along x direction, and spatial distributions of LDOS for $\text{As}_x\text{P}_{1-x}$ monolayers with varied atomic ratios and arrangements.
- [40] W. S. Choi, H. Ohta, and H. N. Lee, *Adv. Mater.* **26**, 6701 (2014).
- [41] H. Miyagawa, S. Koshiba, K. Takao, K. Fujii, M. Mizumaki, O. Sakata, S. Kimura, R. Ueji, and N. Sumida, *Jpn. J. Appl. Phys.* **45**, 3548 (2006).
- [42] S. Datta, *Electronic Transport in Mesoscopic Systems* (Cambridge University Press, Cambridge, UK, 1995).
- [43] D. L. Guo, B. Shao, C. H. Li, and Y. L. Ma, *Superlattices Microstruct.* **100**, 324 (2016).
- [44] Y. B. Chen, Z. Y. Shen, Z. W. Xu, Y. Hu, H. T. Xu, S. Wang, X. L. Guo, Y. F. Zhang, L. M. Peng, F. Ding, Z. F. Liu, and J. Zhang, *Nat. Commun.* **4**, 2205 (2013).
- [45] G. Zhang and Y. W. Zhang, *Mech. Mater.* **91**, 382 (2015).
- [46] W. N. Zhu, M. N. Yogeesh, S. X. Yang, S. H. Aldave, J. S. Kim, S. Sonde, L. Tao, N. S. Lu, and D. Akinwande, *Nano Lett.* **15**, 1883 (2015).
- [47] G. C. Solomon, C. Herrmann, T. Hansen, V. Mujica, and M. A. Ratner, *Nat. Chem.* **2**, 223 (2010).
- [48] Y. Tsuji, R. Movassagh, S. Datta, and R. Hoffmann, *ACS Nano* **9**, 11109 (2015).
- [49] B. Radisavljevic, A. Radenovic, J. Brivio1, V. Giacometti, and A. Kis, *Nat. Nanotechnol.* **6**, 147 (2011).